HiSST: International Conference on
High-Speed Vehicle Science Technology
26–29 November 2018, Moscow, Russia

Numerical simulation assistant design of the near-field sonic boom signature measurement system for AVIC ARI's FL-60 wind tunnel

Leng Yan [1,2], Liu Zhongchen[1,2], Qian Zhansen[1,2,]*

Abstract

In the present paper, we present the design of the near-field sonic boon signature measurement system for AVIC ARI's FL-60 wind tunnel. FL-60 is a trisonic, blowdown wind tunnel. The Mach number range is of 0.3 to 4.2, and the size of the test section is 1.2mX1.2m. For supersonic condition, a 2-D flexible nozzle with deformable contour flat is utilized to realize Mach number 1.3-4.0 continuously. Most of the design works are by virtue of CFD numerical analysis. In the CFD numerical simulation, the hybrid mesh with a combination of tetrahedral and hexahedral grid is utilized with mesh adaptive strategy to improve the grid resolution. A rail pressure measurement equipment is used in the present work to instead of the traditional pressure probe to improve the measurement efficiency drastically. Based on the conditions of the AVIC ARI's FL-60 wind tunnel, the size and location of the pressure rail is optimized by the CFD simulation to get the best measured data. And also the effects of flow non-uniform of the tunnel on the sonic boom data are analyzed numerically. The numerical results show that the pressure rail can give satisfied near-field off-body pressure signatures for the present axisymmetric reference model and that will be validated by the reference model tests in the near future.

Keywords: *sonic boom, wind tunnel measurement, numerical simulation, off-body pressure, FL-60 wind tunnel*

Nomenclature

h – Model height above probe orifice
L – Model length, millimeter
M – Mach number
p_∞ – Freestream static pressure, Pa
p_{rail} – Static pressure from rail orifice, Pa
dp – Differential static pressure ($p_{rail} - p_\infty$), Pa
dp/p_∞ – Overpressure coefficient
h/L – Model height above probe orifice non-dimensionalized by model length

[1] *AVIC Aerodynamics Research Institute, Shenyang, 110034, China.*
[2] *Aviation Key Laboratory of Science and Technology on High Speed and High Reynolds Number Aerodynamic Force Research, Shenyang, 110034, China Affiliation.*
[*] *Corresponding Author. E-mail address: qianzs@avicari.com.cn.*

1. Introduction

Currently, flight at supersonic is not permitted over land for many countries. The primarily reason is the sonic boom annoyance and potential structural damage caused by large pressure waves When the aircraft flights at speeds greater than the speed of sound [1]. It is generally recognized that the sonic boom is one of the most important questions concerning the future of supersonic aircraft, particularly with regard to commercial air transportation. The measurement of the off-body pressure signatures of the low-boom supersonic vehicles modern in wind tunnel is challenging [2-7]. The testing in wind tunnel often provides measurements of the off-body signatures from less than one to several body lengths away from the model. So, the aircraft configuration must be accurately represented at very small scales and the near-field off-body pressure signatures must be measured accurately with minimal interference from the wind tunnel flow field. In addition, the model shock waves must have no distortion between the model and the measuring devices [8].

Historically, the conical probe was used to measure static pressure at a single point in the flow-field when the off-body pressure signatures were measured in a wind tunnel, as shown in the Fig. 1. This technique requires axial translation of the model past the probe or translation of the probe past the model to obtain the whole off-body pressure signatures of the model. The one disadvantage of this single point measure method is time-consuming. For a continuous flow wind tunnel, in order to ensure the data accuracy, the pressure oversampling time has better up to 30 seconds, and the measurement points desired on a model are at least 80~100. The whole run time to the exclusion of the equipment movement is about 50~60 minutes per signature obviously. The other disadvantage of this single point measure method is prone to reduced data accuracy. The tunnel conditions which contribute to reduce data quality (humidity, turbulence, ambient pressure variations and stream angle) change over such long times.

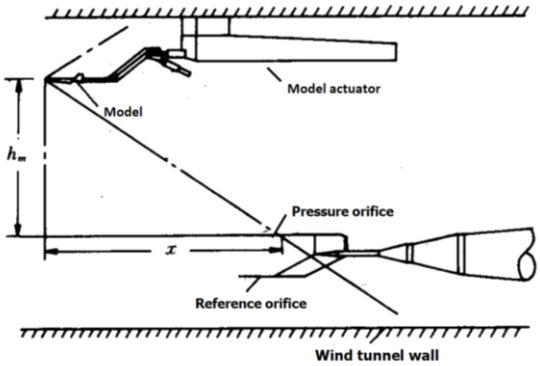

Fig. 1 Wind tunnel apparatus

Ideally, measurement equipment should measure an entire signature all at once. Unlike single-point conical probes, hundreds of pressure orifices which are used to measure a model's entire off-body pressure signature at one location of the model in the wind tunnel are laid on the surface of the pressure rail. Compared with conventional single conical probe, pressure rail has significant advantages in efficiency and precision.

In the present paper, we present the design of the near-field off-body pressure signature measurement system for AVIC ARI's FL-60 wind tunnel. In the CFD numerical simulation, the hybrid mesh with a combination of tetrahedral and hexahedral grid is utilized with mesh adaptive strategy to improve the grid resolution. A pressure measurement rail is used in the present work to instead of the traditional pressure probe to improve the measurement efficiency drastically. Based on the conditions of the AVIC ARI's FL-60 wind tunnel, the size and location of the pressure rail is optimized by the CFD simulation to get the best measured data. The numerical results show that the pressure rail can give satisfied near-field off-body pressure signature for the present axisymmetric reference model, and that will be validated by the reference model tests in the near future.

2. Introduction of AVIC ARI's FL-60 wind tunnel FL-60

FL-60 is a trisonic, blowdown wind tunnel, as shown in Fig. 2. It is composed of butterfly valve, expansion joint, pressure regulating valve, large-angle expansion section, stable section, contraction section, flexible wall nozzle, transonic test section, supersonic diffusion section, ejector, subsonic diffusion section, muffler, etc. The length of the wind tunnel is about 92 meters.

Fig. 2 FL-60 Wind tunnel

The range of Mach number is 0.3 to 4.2, and the size of the test section is 1.2m × 1.2m. For supersonic condition, a 2-D flexible nozzle with deformable contour flat is utilized to realize Mach number 1.3-4.2 undiscretely. The experimental capabilities of FL-60 include conventional force test/pressure test, air intake test, unsteady flow test at high angle of attack, dynamic derivative test, large amplitude oscillation test, external store force test, component force test, hinge-moment test, half model supporting, aeroelasticity simulation, CTS, PSP, TSP, IR, schlieren and etc.

The wind tunnel design indexes are as follows:

(1) Test section size

Transonic: 1.2m × 1.2m × 3.8m (width× height × length)

Supersonic: 1.2m × 1.2m × 2.2m (width × height × length)

(2) Mach number range

Ma=0.3~4.2

(3) Mach number control accuracy

Conventional: $\Delta \mathrm{Ma} \leq \pm 0.005$, when the Mach number is controlled accurately: $\Delta \mathrm{Ma} \leq \pm 0.0015 \ (0.3 \leq \mathrm{Ma} \leq 1.2)$

$\Delta \mathrm{P}_{0\,\max} / \mathrm{P}_0 \leq 0.3\% \ (1.5 \leq \mathrm{Ma} \leq 4.2)$

3. Design of Pressure Rail and test techniques

3.1 Design of Pressure Rail

Pressure rail has the advantage of measuring all the off-body pressure signatures at once, since hundreds of pressure orifices are laid on the surface of it. Although this measurement technique avoids the problem which is need long period of time to take signatures, it introduces other problems. Firstly, the bow shock wave generated by the pressure rail crosses the model shock waves and distorts them, although this phenomenon depends on placement of the rail relative to the model. Secondly, due to the exits of top surface of the pressure rail, the measured data on a rail are magnified by the reflection factor. If the top surface of the pressure rail is an infinitely-thin surface, the reflection factor is 1 which means non-reflective. Similarly, if the top surface is an infinitely-wide flat plate, the reflection factor is 2 which mean non-reflective reflection. Furthermore, the shock reflection of the wind tunnel wall and turbulence boundary layer effect must be considered during measuring off-body pressure signatures.

Based on the theory of static pressure conical probe, the concept of non-reflective pressure rail (RF1) will be realized [9-11]. The RF1 rail has a small rounded tip and is blade-like with a small angle from the tip to the base, and its measurement orifices facing into the flow. Because the upper edge is small (2.54 mm in diameter) and round, it will not has great influence on the flow field to increase measurement amplitude in measurement. The measurement upper edge is transited to 24mm width at its base gradually, and with a 3.5 degree angle from the tip to the base In order to minimize flow disturbance, the cross-section for the whole length need to keep slim. Fig.3 is the cross section of the rail. The rail has a radius tip and is 1.54m long with measured section 1.38m long. The rail height (355.6mm) is selected to prevent turbulence boundary layer effect and contamination of the aft part of a model's signature measured on the rail by reflections off the tunnel wall of model shock waves from the forward part of the model. The RF1 pressure rail consists of 350 pressure orifices spaced 4 mm apart, each with an internal diameter of 0.381mm. Fig.4 is the whole view of the rail.

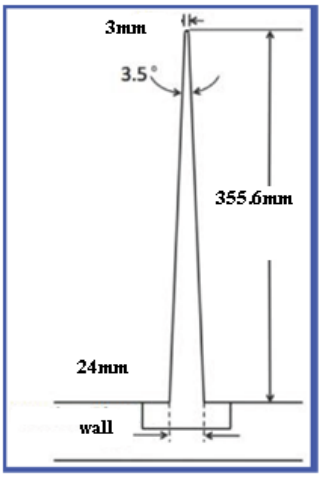

Fig. 3 Cross section of the rail

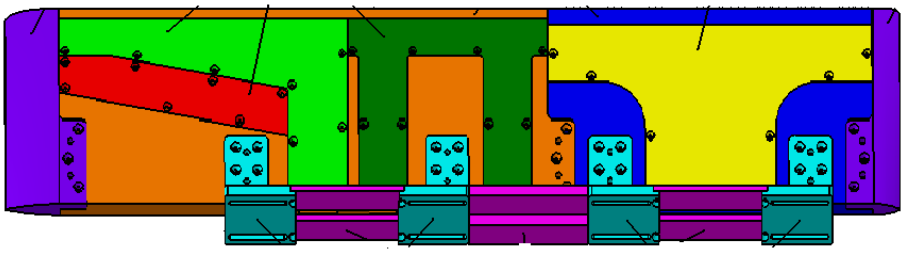

Fig. 4 The whole view of the rail

The RF1 pressure rail based on the above concept has the design attributes as follows:

1). the reflection factor is 1;

2). small circular radius upper edge permits three-dimensional flow;

3). Model shocks reflect from the wall downstream of the measured signatures;

4). Pressures are measured outside the tunnel turbulence boundary layer.

3.2 Reference Run

Another key technique for acquiring sonic boom data using the pressure rail is that the measured data must be corrected with the reference data. The primary purpose is to guarantee that the final data measured only the model's signatures and not the ambient freestream signatures from the tunnel flow. The reference experiment introduces the concept of "clean" wind tunnel. That is, the model and support devices are either out of the wind tunnel during one test (but this is usually not necessary), or the model is moved far enough away from the rail to keep model shocks off the pressure rail or toward the rear of it.

Fig. 5 is the schematic diagram of the model position in the reference and measuring data test. When the model is in the reference test position, the shocks are behind the pressure rail. Accordingly,

when the model is in the measuring position, the shocks fall on the instrumented section of the pressure rail. It is clear that the distance is far enough between measuring data and reference data. It is well known that the disturbance in the supersonic flow field cannot propagate forward, so it will not pollute the measured data. Fig. 6 shows the curve corrected with reference test in ref. 6. The red curve is the reference data, which is the wind tunnel's ambient pressure signatures on the pressure rail, and the black curve is the measured data. The corrected pressure signatures obtained by subtracting the reference signatures from the measured signatures of the model are shown in the figure as the blue curve. From the Fig. 6, it can be seen that this correction method can eliminate the influence of the pressure rail effectively.

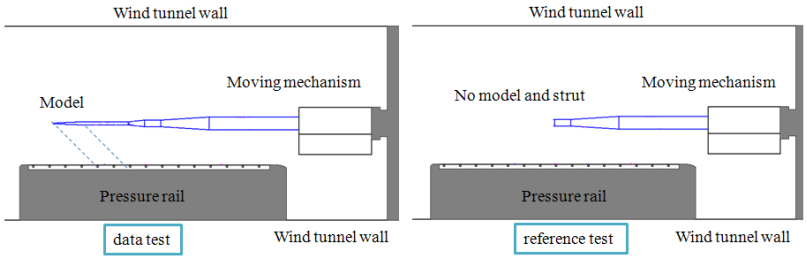

Fig. 5 Layout of reference and data test in FL-60 wind tunnel

Fig. 6 Isolate model pressure signature from rail by reference experiment technique (ref. 1)

4. Computational Results for Pressure Rail

4.1 Model and calculation conditions

The pressure rail must be verified by CFD before manufacture. A low-boom low drag axisymmetric Seeb-ALR model which is designed after the work of Seebass, George and Darden [12] is used as test model. The characteristic length of this model is L=0.2245m. Fig. 7 shows the geometry of the Seeb-ALR model. It is observed that the pressure signatures of this model exist small flat pressure region behind the nose shock. The flat-top pressure signatures have great advantage in revealing and understanding the measurement distortions. According to the wind tunnel test, the calculation conditions are given in table 1. As the relative position of the model and pressure rail is different, the pressure signatures of the model will be located on the different positions of the rail. The next section explain the impact in detail.

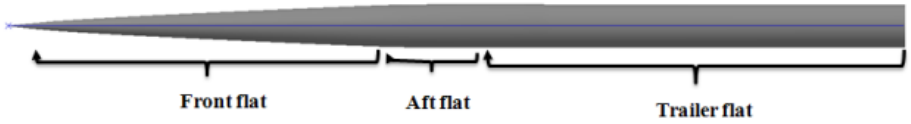

Fig. 7 The geometry of the Seeb-ALR model

Table 1 calculation conditions

case	Ma	static pressure/pa	model	The position of model pressure signature

1	1.8	29978.9	√	B
2	1.8	29978.9	√	A
3	1.8	29978.9	√	C
4	1.8	29978.9	×	×
5	1.5	40021.4	×	×
6	1.5	40021.4	√	B

4.2 Computational Results

Based on the test process, CFD verification is carried out in the following three steps. Firstly, it is to simulate the case without model as the same as the reference correction and to analyze the characteristic of flow field with only the wind tunnel wall and pressure rail in the calculation domain. Secondly, according to the flow field characteristic of the pressure rail, the relative positions between model and pressure rail are divided into three parts (as A,B,C in table 1). The calculation results based on the cases in table 1 will indicate whether meeting the test requirement. Finally, the simulation Mach number is changed to verify the result and law obtained in the second step.

4.2.1 Case4 and case5 Results

This section mainly analyses data of case4 and case5 in table 1. The pressure contours of pressure rail and wall is shown in Fig. 8 and Fig. 9, where the curve is the pressure signature on the upper surface of the pressure rail. It can be seen from the figure that the pressure signature on the upper surface of the pressure rail can be divided into three parts for all Mach number. A is the part affected by the compression region formed by the leading edge of the pressure rail. B is the region undisturbed by strong shock wave. C is the high pressure region formed by reflected shock wave from the wind tunnel wall. The model is located at a certain distance above the pressure rail during the test. The next section will discuss the difference in detail when the pressure characteristic of model is located in these three regions respectively. Furthermore, the CFD verifies whether the design of the pressure rail and reference correction meet the test requirements.

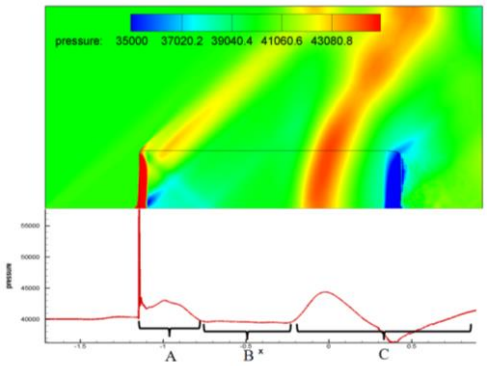

Fig. 8 Pressure contours of pressure rail and wall, case5

4.2.2 Case1 case2 and case3 Results

This section mainly analyses data of case1, case2 and case3 in table 1. The case1 simulation is with the model offset 0.24m downstream of the rail leading edge, and at h=0.22m. The computational result of the model, pressure rail, and tunnel wall is shown in Figure 10. The model crosses the compression region of the rail leading edge, and the pressure signature of the model is located at region B. The model's leading shock reflects from the wall far downstream of the model pressure signature on the rail. In order to obtain accurate signature, an additional computation which is the model in free-field (without the rail and wall) is run in the same position. The pressure signature along the rail is extracted from the three solutions and plotted in Figure11a. Subtracting the rail and wall solution from the model, rail, and wall computation yields the pressure signature of the model. The result compared with the free-field computation is shown in Figure 11b. The computation

shows that the pressure rail provides a good pressure rail design without any indication of reflection from the rail. The reference correction meets the test requirements.

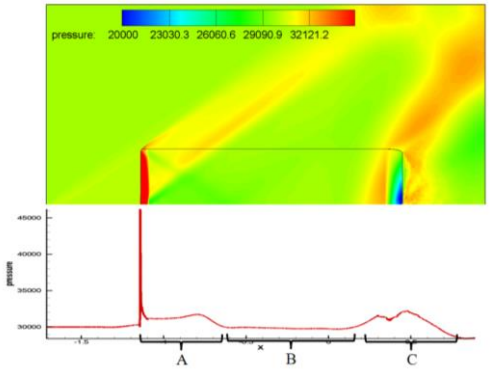

Fig. 9 Pressure contours of pressure rail and wall, case4

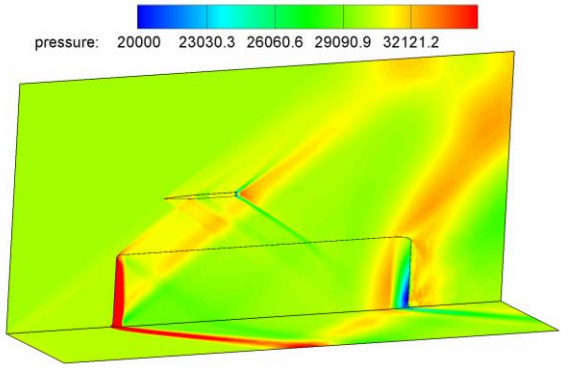

Fig. 10 Pressure contours of the case1

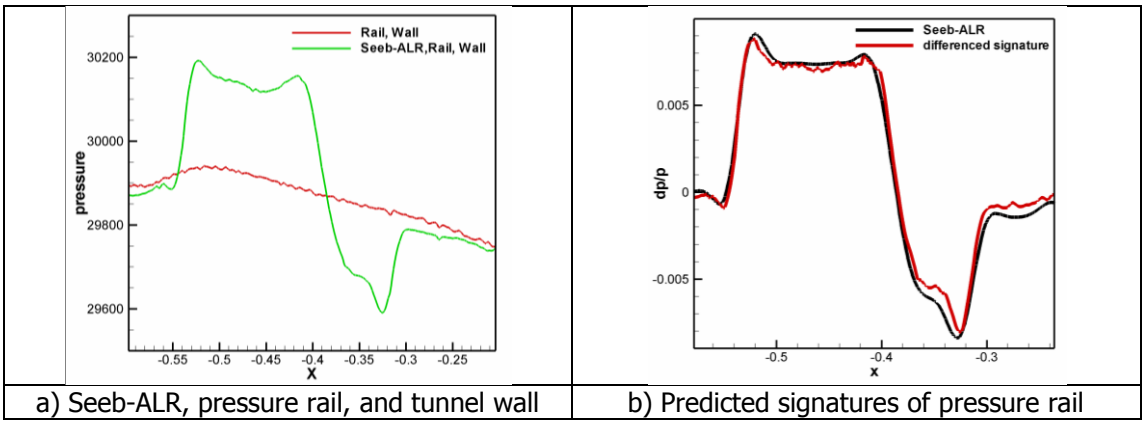

a) Seeb-ALR, pressure rail, and tunnel wall | b) Predicted signatures of pressure rail

Fig. 11 Results of Seeb-ALR, pressure rail, and tunnel wall for case1

The pressure rail is evaluated for different flow direction relative position to model. The computational simulation (case2 and case3) is with the model offset 0.015m upstream and 0.785m downstream of the rail leading edge respectively, while the vertical position remains unchanged. The computational result of the model, pressure rail, and tunnel wall is shown in Fig. 12 and Fig. 13. The pressure signature of the model is located at region A and C respectively. The pressure signature along the rail is extracted from the solutions and plotted in Fig. 13 and Fig. 14. It can be seen from figures that the two cases cannot obtain satisfactory results even if reference correction is introduced. For case2, the shock waves emitting from the model are exactly within the influence range of the leading compression region, so the data accuracy is greatly affected. For case3, the shock waves emitting from the model are exactly within the influence range of the reflection shock wave, and the data accuracy is affected as same. According to the calculation results, it is found that the model shock waves is best located in the central part (part B) of the pressure rail during wind tunnel test.

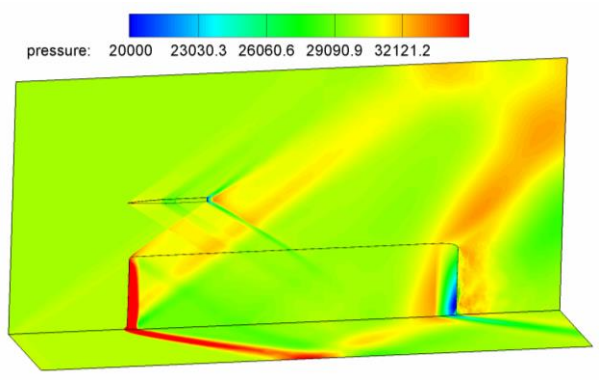

Fig. 12 Pressure contours of the case2

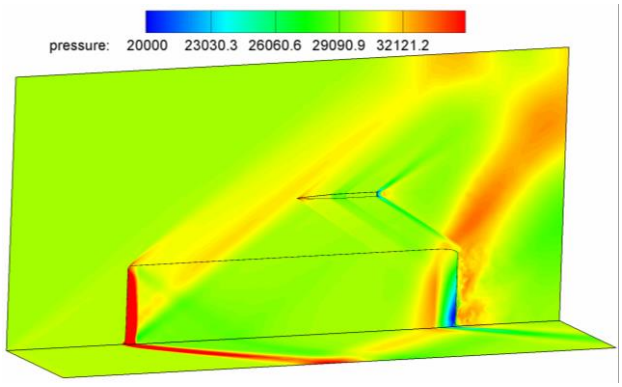

Fig. 13 Pressure contours of the case2

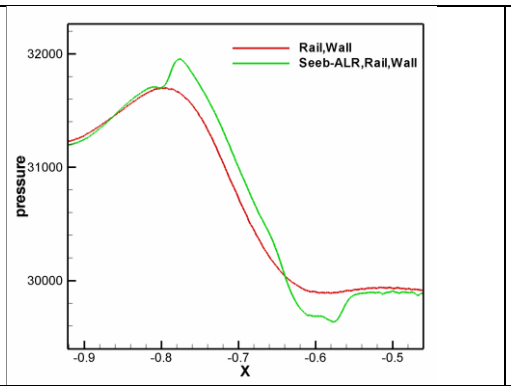

a) Seeb-ALR, RF1 rail, and tunnel wall

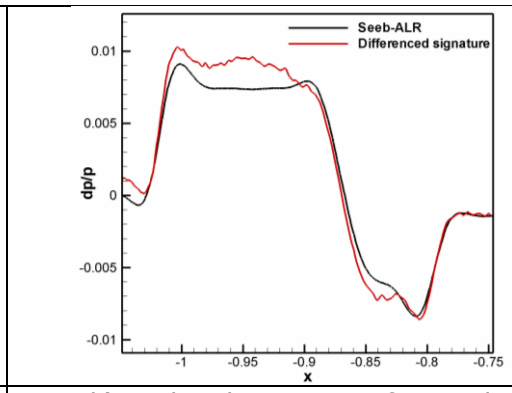

b) Predicted signatures of RF1 rail

Fig. 14 Results of Seeb-ALR, pressure rail, and tunnel wall for case1

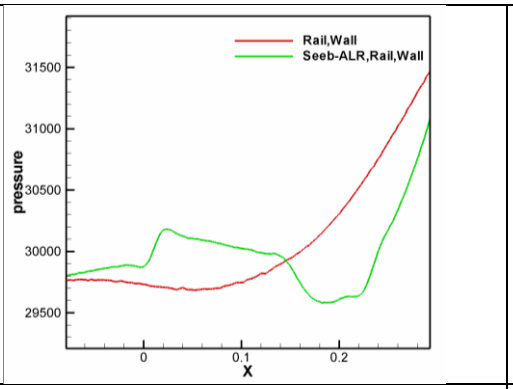

a) Seeb-ALR, RF1 rail, and tunnel wall

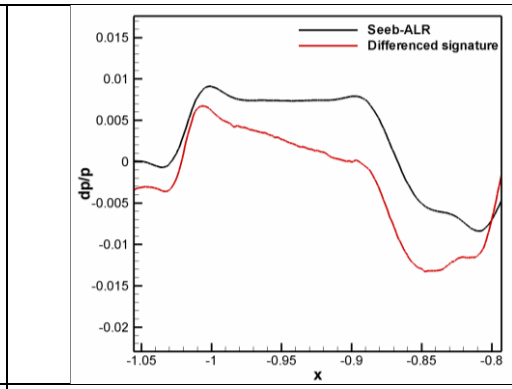

b) Predicted signatures of RF1 rail

Fig. 15 Results of Seeb-ALR, pressure rail, and tunnel wall for case1

4.2.3 Case6 Results

It can be seen from the above analysis that the pressure rail meets design requirements including no-reflection and avoiding boundary layer effect. When the model signatures are located in the part B of the pressure rail, the wind tunnel test requirement can be obtained by introducing the reference correction. The above conclusion is verified by case6.

The computational result of the model, pressure rail, and tunnel wall is shown in Figure 16. The pressure signature along the rail is extracted from the three solutions and plotted in Figure17a. Subtracting the rail and wall solution from the model, rail, and wall computation yields the pressure signature of the model. The result compared with the free-field computation is shown in Figure 17b. The computation shows that the pressure rail provides a good pressure rail design without any indication of reflection from the rail, which further validates the conclusions obtained in section 4.2.2.

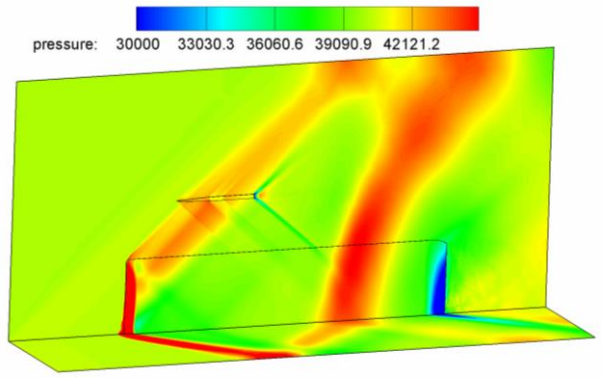

Fig. 16 Pressure contours of the case6

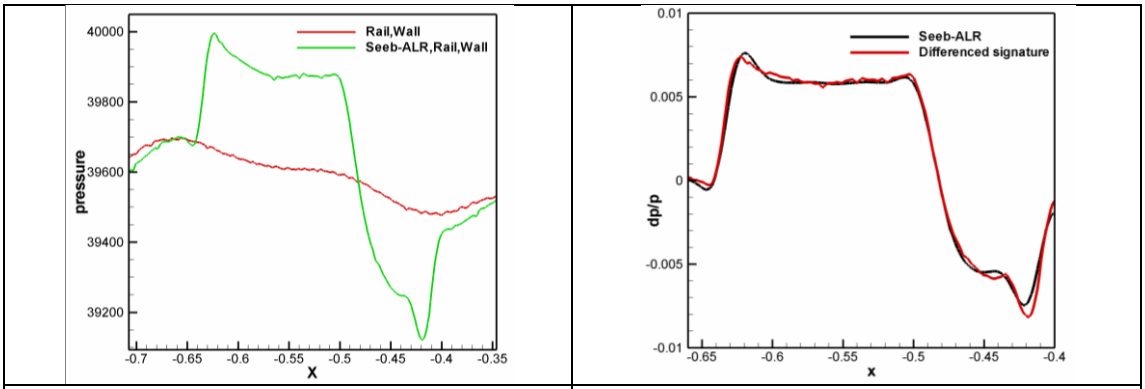

a) Seeb-ALR, RF1 rail, and tunnel wall | b) Predicted signatures of RF1 rail

Fig. 17 Results of Seeb-ALR, pressure rail, and tunnel wall for case1

5. Conclusion

In the present paper, we present the design of the near-field sonic boom signature measurement system for AVIC ARI's FL-60 wind tunnel. A pressure measurement rail is used in the present work to instead of the traditional pressure probe to improve the measurement efficiency drastically. The size and location of the pressure rail is optimized by the CFD simulation to get the best measured data. The numerical results show that the pressure rail provides a good pressure rail design without any indication of reflection from the rail. The FL-60 can give satisfied near-field sonic boom signature for the present axisymmetric reference model.

References

1. Donald A. Durston, Alaa A. Elmiligui, Susan E. Cliff, Courtney S. Winski, Melissa B. Carter, and Eric L. Walker: Experimental and computational sonic boom assessment of Boeing N+2 low boom models. AIAA 2014-2140.

2. Mack R. J., An Analysis of Measured Sonic-Boom Pressure Signatures From a Langley Wind-Tunnel Model of a Supersonic-Cruise Business Jet Concept, NASA TM-2003-212447.
3. Graham D. H. and Dahlin J. A., Wind Tunnel Validation of Shaped Sonic Boom Demonstration Aircraft Design, AIAA 2005-7.
4. Mack R. J., Method for Standardizing Sonic-Boom Model Pressure Signatures Measured at Several Wind-Tunnel Facilities, NASA TM-2007-21485.
5. Furukawa T., Makino Y., Noguchi M. and Ito T., Supporting System Study of Wind-Tunnel Models for Validation of Aft-Sonic-Boom Shaping Design., AIAA 2008-6596.
6. Elmiligui A., Wilcox F., Cliff S., and Thomas S., Numerical Predictions of Sonic Boom Signatures for a Straight Line Segmented Leading Edge Model. Seventh International Conference on Computational Fluid Dynamics (ICCFD7) Big Island, Hawaii, July 9-13, 2012.
7. Wilcox F. J., and Elmiligui A.A., Experimental Sonic Boom Measurements on a Mach 1.6 Cruise Low-Boom Configuration, NASA, TM-2012-217598.
8. Donald A. Durston and Susan E. Cliff: Near-field sonic boom test on two low-boom configurations using multiple measurement techniques at NASA Ames. AIAA 2011-3333.
9. John M. Morgenstem: How to accurately measure low sonic boom or model surface pressures in supersonic wind tunnels. AIAA 2012-3215.
10. S. Cliff, A. Elmiligui, M. Aftosmis, S. Thomas, J. Morgenstern, D. Durston: How to accurately measure low sonic boom or model surface pressures in supersonic wind tunnel. ICCFD7-2006.
11. John M. Morgenstern: Distortion correction for low sonic boom measurement in wind tunnels. AIAA 2012-3216.
12. George, A. R., and Seebass, R., "Sonic Boom Minimization Including Both Front and Rear Shocks," AIAA J. Vol. 9, No.10, Oct. 1971, pp. 2091-2903.